Hindawi
International Journal of Antennas and Propagation
Volume 2018, Article ID 5016847, 13 pages
https://doi.org/10.1155/2018/5016847

Research Article

Proficiency of Leaky Coaxial Cable-Based MIMO System Using Radiated Field Distribution

Asad Saleem[1], **Fangqi Zhang**[2,3], **Min Wang**[1], **Xiaoyu Yin**[1], **and Guoxin Zheng**[1]

[1]*Key Laboratory of Specialty Fiber Optics and Optical Access Networks, Joint International Research Laboratory of Specialty Fiber Optics and Advanced Communication, Shanghai Institute for Advanced Communication and Data Science, Shanghai University, 200444 Shanghai, China*
[2]*The Key Laboratory of Road and Traffic Engineering, Tongji University, Ministry of Education, Shanghai 201804, China*
[3]*Maglev Transportation Engineering R&D Center, Tongji University, Shanghai 201804, China*

Correspondence should be addressed to Guoxin Zheng; gxzheng@staff.shu.edu.cn

Received 7 August 2018; Revised 15 October 2018; Accepted 30 October 2018; Published 31 December 2018

Academic Editor: Xianming Qing

This paper presents channel propagation characteristics of different multiple-input multiple-output (MIMO) systems using ray tracing approach in a confined area at 1.8 GHz according to the LTE-M standards. Leaky coaxial cables were exploited at different transmitted locations to visualize the fluctuated radiated field under different polarization combinations. In order to encounter this vision, the reflected and line-of-sight paths are under consideration for both vertically and horizontally polarized waves emitting from the leaky coaxial cables (LCXs). Emphasis is given to understand the effect of LCX configuration on the channel correlation coefficient and capacity (C) in the confined area. The exploration of experimental results reveals that the MIMO channel using LCXs has significant performance, specifically in the case of horizontal polarization. Furthermore, it is inferred that for the longer distance between transmitter and receiver, the correlation coefficients have higher magnitude.

1. Introduction

Long-Term Evolution for metro technology is well-known as the stable communication approach for advanced urban rail transit system due to the few drawbacks of the wireless local area networks (WLANs) in the communication-based train control (CBTC) systems. The important findings for the LTE-M are improved spectral efficiency and high data rates communication. LTE-M utilizes LCX for reliable and long-term communication in underground tunnels, subways, malls, etc. [1, 2]. In confined areas, the electromagnetic waves' attenuation gets serious after many reflection and scattering times when the conventional antenna is used. The antenna parameters and radiation characteristics have significant effects on field coverage [3]. Leaky coaxial cables have been exploited for many years due to their enormous advantages for indoor environment over conventional antennas such as ensuring limited interference among cells, steady coverage, and easy installation [4]. LCXs have basically uniform linear slotted array with a fixed-phase delay among two neighboring slots, and the slots are supposed to be cut down in the infinite metal plane which has negligible effects on the field scattering [5].

Due to supplementary degree of freedom provided by the spatial multiplexing, multiple-input multiple-output (MIMO) technology is recognized as a promising technique to achieve higher spectral efficiency. In [6, 7], two independent LCXs were used to configure a 2×2 LCX MIMO system for corridor scenario, and it was found that LCX is favorable for indoor environment communication and the performance of the MIMO channel is closer to an i.i.d. channel. The finite-difference time-domain (FDTD) method is used to calculate the radiated field of cylindrical coordinates accurately. In [8], the coupling losses and the different slot configuration were discussed impressively. The far field was acquired by integrating the radiated field in the slots aperture which was systematized through the dyadic Green's function. Ray tracing (RT) method is generally used for detailed

prediction of radio channel constraints and precision of near-field computations for confined areas. In the tunnel environment, the material of the walls affects the radiation pattern emitted from the LCX. The diffuse scattering in the ray tracing simulations significantly cuts down the root mean square (RMS) prediction inaccuracy [9]. RT prediction technique delivers precise results when detailed system configurations and environment models are deliberated [10]. A feasible paradigm was realized for understanding the realistic high-speed train (HST) channels at the 5 G mm wave band [11], and the key propagation phenomena were approximated through extensive RT simulations. The vehicle-to-vehicle- (V2V-) based communication at 5 GHz band for the line-of-sight track between Tx and Rx under different realistic environments (such as traffic signs, buildings ground, and lampposts) was obstructed through RT simulations, and it was found that higher antenna distribution can attain improved coverage with smaller path loss (PL) than lower antenna distribution in the presence of obstructed vehicles [12].

The influence of signal correlation on the 2×2 MIMO system performance was investigated in [13]. It was found that correlation depends on the phase of the wave, the number of Rx and Tx antennas. It was also inferred that the correlation of 0.5 has an obvious influence on the MIMO performance. The description of capacity evaluation of LCX MIMO system using single LCX was examined using water filling power allocation scheme and equal power distribution scheme and the results were further compared with the conventional LCX MIMO systems. It was then found that the proposed system shows efficient performance in terms of capacity at 2.4 GHz and 5 GHz bands [14]. Though the literature provides numerous studies, most of these studies have insufficiency of experimental validations of analytical results.

Since there exists an enormous interest for the MIMO system deployment for the LTE-M system in the tunnel environment, we propose a radiated model for the different MIMO channels at 1.8 GHz. For measurement campaign, LCXs with the vertical and horizontal polarizations are considered, which are laid parallel to each other at some finite distance from the receiver. For evaluating the feasibility of MIMO channel, radiated field from LCXs is examined for the scattered (NLOS) and the line-of-sight (LOS) paths. Moreover, the correlation coefficients and channel capacities are investigated for different MIMO systems. We found that the MIMO system using LCX deployment in a confined area has favorable performance in terms of higher capacity and lower correlation. The paper is organized as follows. Section 2 determines the radiated field description using cylindrical coordinates. Section 3 describes the measurement configuration, and Section 4 depicts the measurement results. Finally, Section 5 concludes the paper.

2. Scattered Field Description

The procedure of computing the scattered radiated field of slots on the conductor sheet is very complex. When one side of the leaky coaxial cable is associated to the source, the transversal radio waves propagating within the cable diffuse from the continuous slots. The transverse proportion has insignificant impact compared to the wavelength, and the radiations from the respective slot are equivalent to the individual magnetic dipole in a free space. In this paper, we considered the horizontally and vertically polarized LCXs. The length of LCX is regarded as L while the length and width of the slot are l and w, respectively. The slot angle is assumed as $2a$, and the inner and the outer radius of cylinder are a and b, correspondingly, as shown in Figure 1(a).

The LCXs are located along z-axis, and the slots of the LCXs are perpendicular to the z-axis. The distribution of the radiated field on the outermost conductor of the LCX along z-axis is validated as [15–18] follows:

$$E_z(\varphi, z) = \frac{V}{w}\left(1 - \frac{\cos(k_0 b\varphi)}{\cos(k_0 b\alpha)}\right), \tag{1}$$

where $V = (-jV_0\sqrt{\varepsilon_r})/[2k_0 b \ln(b/a)]$, φ is the angle between r' and the x-axis, and θ is the angle between r and the z-axis. Distance from point o to one point in space is r whose projection in xoy plane is r' as shown in Figure 1(b). Since the width of the slot is negligibly small, hence the radiated field is assumed as constant. The circumferentially electric field is defined as follows:

$$E_\varphi = V(\theta, \varphi)\frac{e^{-jk_0 r}}{r}\sin\theta, \tag{2}$$

where

$$V(\theta, \varphi) = \frac{jV\cos\theta}{\pi^2 bk_0 \sin^3\theta}\sum_{n=-5}^{n=+5}\frac{ne^{jn\varphi}j^{n+1}}{H_n^{(2)\prime}(bk_0\sin\theta)} \cdot \left(\frac{\sin n\alpha}{n} - \frac{m\sin m\alpha\cos n\alpha - n\cos m\alpha\sin n\alpha}{(m^2 - n^2)\cos m\alpha}\right), \tag{3}$$

where $m = k_0 b$, ϵ_0 is the dielectric coefficient of free space, ω is the angular frequency, and H_n^2 is the Hankel function of the second type of n-th rank. By using the ray tracing approach, the E_y which is the vertically polarized quantum of E_φ is given below:

$$E_y = V(\theta_i, \varphi_i)\frac{e^{-jk_0(r_i + r_{i1}) - j\beta_i P}}{r_i + r_{i1}}\sin\theta_i\cos\varphi_i\Gamma_v, \tag{4}$$

where

$$r_i = \sqrt{x_0^2 + h_0^2 + z_0^2},$$

$$r_{i1} = \sqrt{x_0^2 + (h - h_0)^2 + (ip - z_0)^2},$$

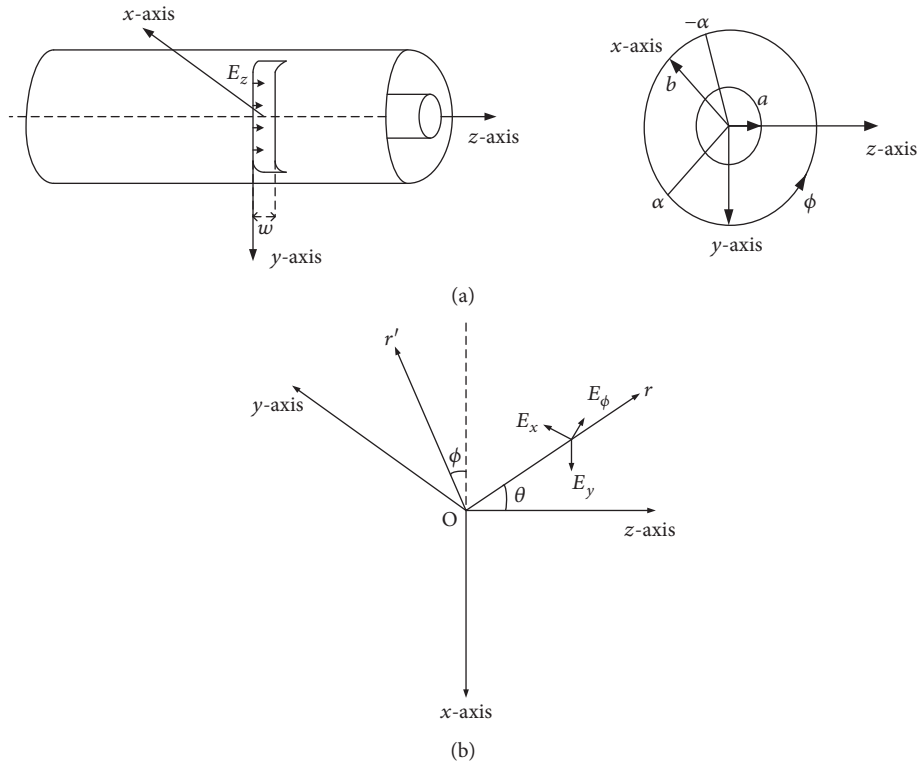

Figure 1: The slot structure of LCX (a). The radiated field of LCX (b).

$$\varphi_i = \arccos\left(\frac{x_0}{\sqrt{{x_0}^2 + {h_0}^2}}\right),$$

$$\theta_i = \arctan\left(\frac{\sqrt{{x_0}^2 + {h_0}^2}}{z_0}\right),$$

$$\beta = k_0\sqrt{\epsilon_r},$$

$$\gamma = \arctan\left(\frac{x_0}{\sqrt{{z_0}^2 + {h_0}^2}}\right), \tag{5}$$

where i is the number of slots, p is the period of slots, x_0 is the distance in the horizontal direction between the left metope of the space and the cable, h_0 is the vertical distance among the cable and incident point, and z_0 is longitudinal distance amongst the cable and the incident point. The reflection coefficient of the vertically polarized waves emitted from the LCX can be written as follows:

$$\Gamma_v = \frac{\left(\epsilon_1 - j{\epsilon_1}'\right)\sin\gamma - \sqrt{\left(\epsilon_1 - j{\epsilon_1}'\right) - \cos^2\gamma}}{\left(\epsilon_1 - j{\epsilon_1}'\right)\sin\gamma + \sqrt{\left(\epsilon_1 - j{\epsilon_1}'\right) - \cos^2\gamma}}, \tag{6}$$

where $(\epsilon_1 - j{\epsilon_1}')$ is the complex dielectric coefficient of the tunnel material and Γ_v is the vertically polarized reflection coefficient. The reflection coefficient of the horizontally polarized LCX is demonstrated as the following:

$$\Gamma_h = \frac{\sin\gamma - \sqrt{\left(\epsilon_1 - j{\epsilon_1}'\right) - \cos^2\gamma}}{\sin\gamma + \sqrt{\left(\epsilon_1 - j{\epsilon_1}'\right) - \cos^2\gamma}}. \tag{7}$$

The entire radiated field is acquired by accumulating the effects of all individual slots of the whole LCX

$$E_{Y\sum} = \sum_{i=1}^{N} V(\theta_i, \varphi_i)\frac{e^{-jk_0(r_i + r_{i1}) - j\beta_i P}}{r_i + r_{i1}}\ \sin\theta_i \cos\varphi_i \Gamma_v. \tag{8}$$

3. Measurement Setup Configuration

The time-domain pseudonoise (PN) sequence correlation technique was assumed in the measurements. Keysight E8267D vector signal generator (VSG) constitutes the transmitter (Tx), and it generates a BPSK signal modulated by PN sequence of 511 chips. The chirp rate was considered as 40.8 MHz which was the same as the transmitted signal bandwidth. The signal is fed to one side of the LCX, and a 50-ohm load was attached to the other port. For the receiver side, a dipole antenna was associated with the R&S FSG spectrum analyzer. The measurement setup configuration is shown in Figure 2. The received signal which constitutes the information regarding phase and amplitude is stored in

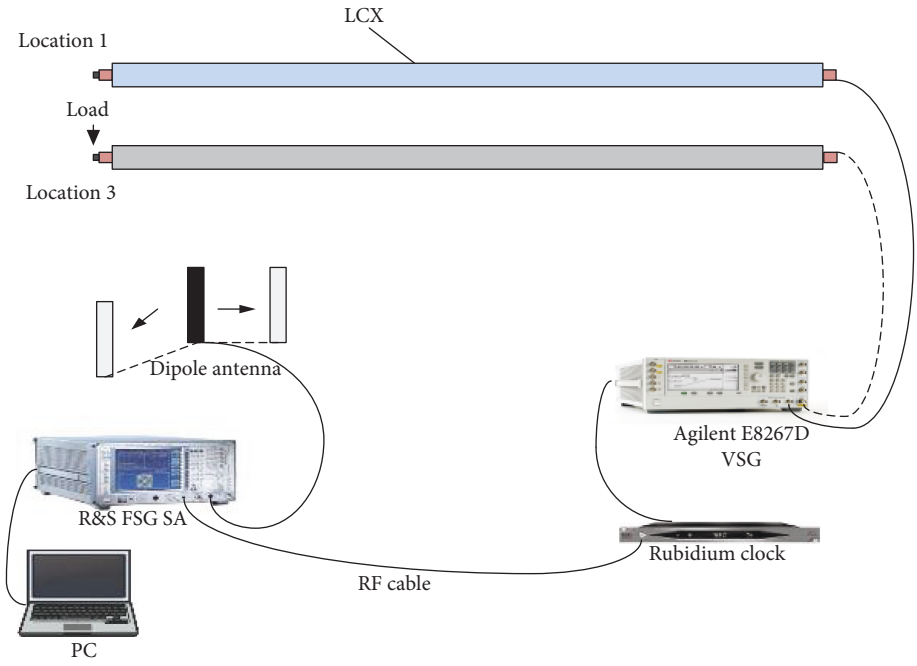

Figure 2: The measurement setup sketch.

a disk array via an Ethernet port in the PC. The rubidium clock source was connected to the transmitter, and the system clock of the receiver was used to preserve phase synchronization. At the end, 4100 channel impulse responses (CIRs) were acquired for every individual measuring point. The measurement campaign was conducted in a vacant subway-like tunnel at Zhongtian Technology Company (ZTT), Nantong, China, which is particularly operated for radiated field measurements. The tunnel is 100 m long, and it consists of two sections: the first section is a 50 m long arched tunnel and the other one is a 50 m long rectangular tunnel. The tunnel walls were shielded with concrete material. The tunnel inner view is given in Figure 3, and the fixed parameters configurations are listed in Table 1. We selected the 50 m long rectangular tunnel for our experiments. The LCXs were laid along the z-axis in the tunnel; the distance between the LCX and receiver was considered along the x-axis and the height from the ground was taken along the y-axis. The volume of the rectangular tunnel is calculated as 50 m (length) × 4.4 m (width) × 3 m (height). The radiuses of the inner and outer conductors of the leaky coaxial cable are given as 6 mm and 16 mm, respectively. The least distance between LCXs and the Rx was calculated as 2 m, and there was nobody moving throughout measurement procedure. Three locations along the walls were considered for electromagnetic measurements through LCX deployment such as Loc1, Loc3, and Loc5. The heights of Loc1, Loc3, and Loc5 from the ground were fixed as 2.7 m, 1.9 m, and 1.5 m, respectively. The frequency was fixed as 1.8 GHz because this frequency delivers strong LTE coverage for an indoor environment.

We divided the total rectangular tunnel into three regions, and each region constitutes a rectangular grid of measurement points (3 × 5) which were marked to attain channel characterization. Here, we acquired total number of 12 (3 × 4) receiving antenna arrays for each region, where d_1, d_2, and d_3 are the distances from LCXs to the first 4 receiving antenna arrays, the middle 4 virtual receiving antenna arrays, and the last 4 virtual receiving antenna arrays, respectively, as specified in Figure 4. The distance between LCXs and the side wall is 0.2 m. The virtual antenna array method was used for measurements, and the minimum distance between two consecutive receiving locations was fixed as 0.5 m. Each region is 2 m longer while region 1 starts from 0 m to 2 m, region 2 consists of 24 m–26 m, and region 3 consists of 48 m–50 m in the rectangular tunnel. In the start of the tunnel near entering the door, there were many metal boxes (near region 1) which reflect many multipaths. Towards the other side of the rectangular tunnel before entering into an arch tunnel, the concrete wall occupies some additional area more than region 1 and region 2. In order to estimate the polarization performance of the MIMO channel, two different kinds of commercial LCXs fabricated by ZTT were exploited.

The first LCX was vertically polarized (periodic slots were directed obliquely), and the other type of LCX was horizontally polarized (periodic slots were directed perpendicular to the LCX axis). As compared to the conventional antennas, LCXs can provide more predictable and homogeneous signal strength for indoor environment. The relationship between different virtual receiving antenna arrays and the analytical received power by considering LOS path only for the horizontally polarized 2 × 2 MIMO system in region 1 is given in Figure 5. The results reveal that the distance has significant impact on the received power for different receiving locations. With the increment of distance between Tx and

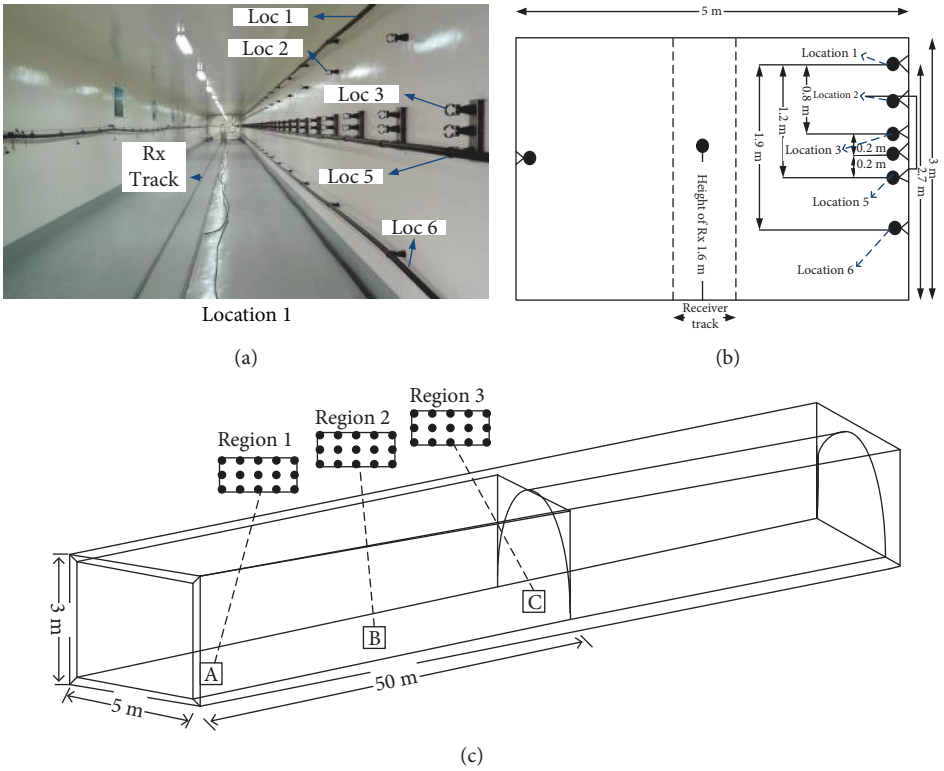

Figure 3: The inner view of the Nantong tunnel (a, b). Tunnel construction in the wireless InSite software (c).

Table 1: Measuring parameters.

Unit	Parameter
Carrier frequency	1.8 GHz
Transmitted power	20 dBm
Bandwidth	40.8 MHz
Tx-antenna	ZTT-LCX of 50 m length
Rx-antenna	UHA9125D dipole antenna
Antenna gain	2.15 dBi
Height of LCX at location 1	2.7 m
Height of the Rx antenna	1.6 m
LCX spacing	Loc1 and Loc3, 0.8 m
LCX spacing	Loc1 and Loc5, 1.2 m
LCX spacing	Loc3 and Loc5, 0.4 m
Slot period of LCX	0.6 m
Sampling rate	81.6 MHz
Resistance	50 ohms
Measurement time	50 ms

the receiver, the correlation increases [19]. According to [20], the effect of antenna polarization on path loss was found to be dependent on antenna position. Horizontal polarization resulted in less path loss when the antennas were mounted close to the ceiling than the vertical polarization. As Loc1 and Loc3 are closer to the ceiling, they have higher received power as compared to the other combinations for the consideration of LOS path.

4. Results Analysis

To understand the LCX-based MIMO channel performance, we considered two properties such as channel correlation coefficients and channel capacity.

4.1. Correlation Coefficients of the MIMO Channel. The appropriate condition for the MIMO channel efficiency is the existence of orthogonal subchannels. The degree of independence of the subchannels can be tested through the correlation analysis. The computation technique for the correlation of the MIMO channel gains from two independent transmitters with the same receiving antenna is discussed comprehensively in [21–23].

The l-th path transmitter correlation between the transmitter antenna elements i and both transmitting to the same mth receiving antenna array element is calculated using the following:

$$t_{ij}^{\mathrm{Tx}} = \frac{E\left[h_{im}h_{jm}^{*}\right] - E[h_{im}]E\left[h_{jm}^{*}\right]}{\sqrt{\left(E\left[|h_{im}|^2\right] - |E[h_{im}]|^2\right)\left(E\left[\left|h_{jm}\right|^2\right] - \left|E\left[h_{jm}\right]\right|^2\right)}}, \tag{9}$$

where $E[.]$ is the expected value operator and t_{ij}^{Tx} denotes the correlation for the channel associated with the i-th and j-th

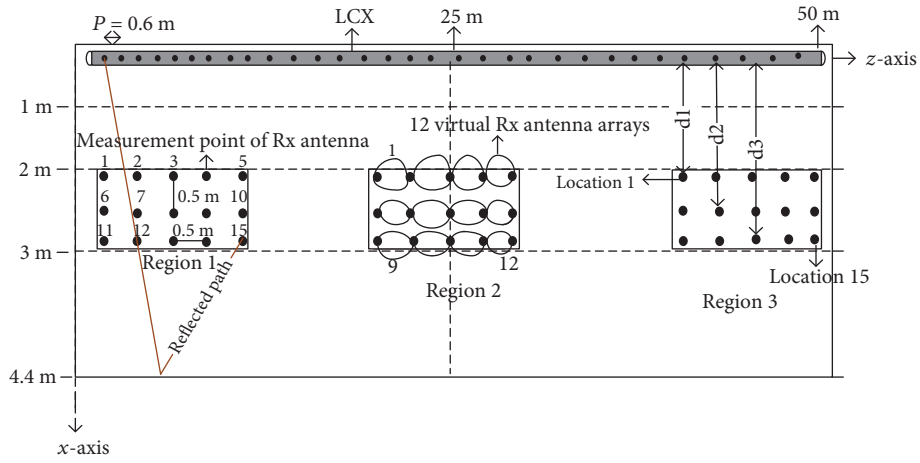

Figure 4: The virtual antenna array view of the Nantong tunnel.

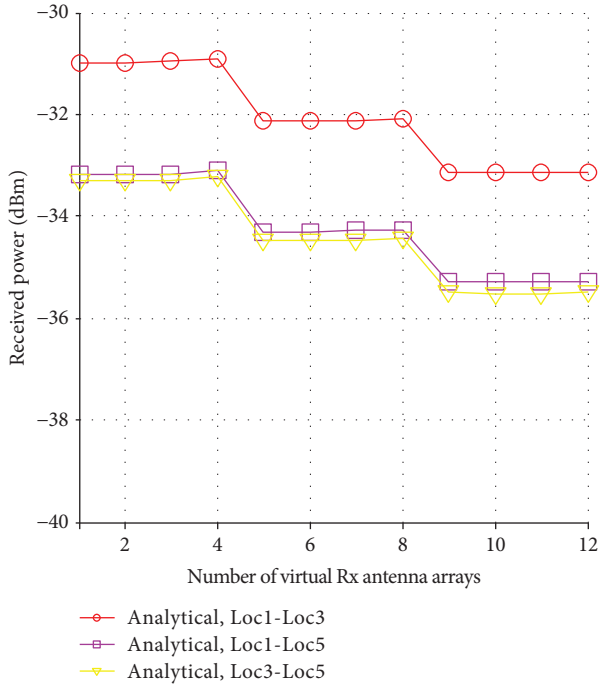

Figure 5: The received power for horizontally polarized LCX MIMO system in region 1.

transmitting elements, and both linked with the same m-th receiver. h_{im} is considered as the channel complex gain between the m-th receiver and the i-th transmitter, and h_{jm} is the channel complex gain between the m-th receiver and the j-th transmitter.

The spatial correlation coefficients' relation with the virtual antenna array for 2×2 LCX MIMO systems by analyzing vertically polarized LCXs and horizontally polarized LCXs are shown in Figure 6. We conceived three locations as Loc1, Loc3, and Loc5 of LCX deployment for the measurements, and we divided it into three different combinations as Loc1-Loc3, Loc1-Loc5, and Loc3-Loc5 to examine the 2×2 MIMO systems. Here, we compared the analytical results with real-time Nantong tunnel experimental results for both LOS and reflected paths, and the reflected path consists of the reflections from walls, roof, and floor of the tunnel. As expected, the transmitter correlation increases as the distance between the transmitter and the receiver arrays increases and vice versa. Despite the LOS propagation consideration in the Nantong tunnel, the correlation magnitude is relatively high. As can be seen from Figure 6, in region 1, for vertical and horizontal polarization, the correlation coefficients have the least value than the other regions. According to [24], the best performances in terms of correlation and capacity can be achieved when the antennas are distributed perpendicular to the middle (center line) of the tunnel due to the maximum number of multipath. So, on the basis of larger distances from the center of tunnel, the correlation also varies. In Figure 6, it is obvious that horizontally polarized LCXs show improved performance in terms of correlation than the vertically polarized ones. The plane wave Fresnel reflection coefficients for reflections on nonperfectly conducting surfaces for both horizontal polarization and vertical polarization are briefly discussed in [25]. The vertical polarization coefficients increase with the incidence angle. But horizontal polarization coefficients have a Brewster angle and are always lower than the vertical polarization coefficients. For horizontally polarized signals, the incident ray on the tunnel floor and ceiling is horizontally polarized but vertical polarization is perceived on the tunnel walls. For vertically polarized signals, the inverse case is conceived. According to the reflection coefficients, the reflected ray power on the tunnel walls for the horizontal polarization is greater than that for vertical polarization. Because of the tunnel height which is smaller than the tunnel width, the reflected rays with the tunnel walls have greater angle of arrival (AOA) than that with the tunnel floor and ceiling. This results in a larger angular spread for horizontal polarization than for the vertical polarization. So, the horizontally polarized configuration has smaller correlation coefficient than the vertically polarized configuration. The additional part of the concrete wall at the end of region 3 causes more reflections of multipaths as compared to the mid of the 50 m long rectangular tunnel (region 2).

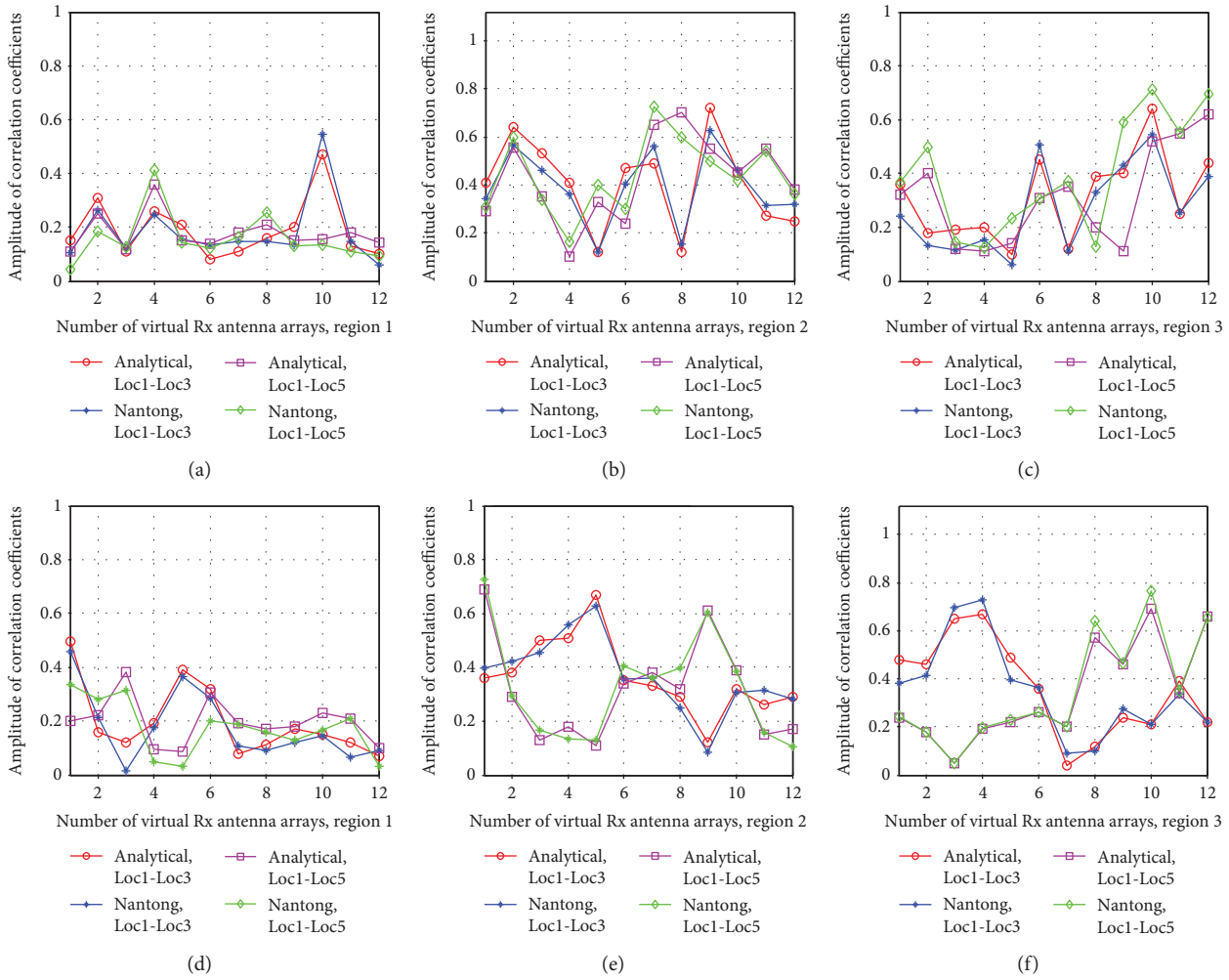

FIGURE 6: The correlation coefficients comparison for 2×2 LCX-based MIMO systems for vertically polarized LCXs for region 1, region 2, and region 3 (a–c) and for horizontally polarized LCXs for region 1, region 2, and region 3 (d–f).

As metals have the tendency to reflect more multipaths than concrete material, so, in region 1, the received signals have less correlation coefficient than other regions. It is also found that region 2 has maximum correlation coefficients than other regions. LCXs can be considered as distributed antenna arrays, and the receiver attains the signals radiated from all aligned slots of the LCXs, and then these signals pass through the subchannels. Therefore, the distribution of the angle of arrivals (AOAs) is decided by accumulating the entire subchannels. The different incident directions of the radiated signals enlarge the angular spread, which is appropriate to deliver the decorrelation of the MIMO channel.

4.2. Channel Capacity Estimation. In practice, the MIMO channel capacity (C) does not depend only on channel multipath but also on the overall received power and the average signal-to-noise ratio (SNR) through the channel. The following two important aspects are generally not independent and approximately some compromise needs to be practiced.

Assuming equal power is transmitted throughout all transmitters and no channel state information (CSI) is available at the transmitter but developed perfectly at the Rx, then the capacity of the 2×2 MIMO channel can be calculated as follows [26–28]:

$$C = \log_2 \det \left[I_{N_R} + \frac{\rho}{N_T} H_{\text{nor}} {H_{\text{nor}}}^H \right], \tag{10}$$

where ρ is the average SNR, N_R and N_T are the number of receivers and transmitters, respectively, $(.)^*$ denotes the Hermitian transpose of a matrix, and I is the identity matrix of size $N_R \times N_R$. In order to eliminate the influence shadow fading, power normalized scheme with the constant SNR is considered first. It is a common practice for antenna design in MIMO systems to normalize H-matrices, so that the average SNR at the Rx elements is adjusted to a fixed value and can be adapted as a parameter. The

complex normalized channel matrix H for each channel realization is given as [29]

$$\mathrm{H}_{\mathrm{nor}} = \mathrm{H}\sqrt{\frac{N_T N_R}{\|\mathrm{H}\|_{\mathrm{F}}{}^2}},$$
$$\|\mathrm{H}\|_{\mathrm{F}} = \sqrt{\sum_{i=1}^{N_R}\sum_{i=1}^{N_T}\left|h_{ij}\right|^2}, \tag{11}$$

where $\|\mathrm{H}\|_{\mathrm{F}}$ is the Frobenius norm of matrix.

As a result, the capacity of the MIMO channel can be achieved by considering the effects of all measurement points in each local region.

4.3. Wireless InSite Ray Tracing Model. Wireless system engineering (WiSE) is a software-based system that calculates both outdoor and indoor radio channel characteristics using ray tracing method. Wireless InSite provides few antenna patterns, for example, half-wave dipole, Lambert's law, automatic, and isotropic [30, 31]. For the indoor version, floors and walls are considered as layered dielectric structures. Transmission and reflection coefficients are measured as requirement, using multilayered structure of Fresnel's formulas. The vector-type nature of the radiated field was not completely assumed; the magnetic field was estimated parallel to the ceilings and floors, then the radiated field was anticipated parallel to all walls for the current WiSE version as shown in Figure 3(c). In principle, each ray between any receiver and the transmitter can be traced efficiently, irrespective of the number of reflections and transmissions. In order to further explore the radiated field characteristics in the tunnel environment, 50 m long LCXs with periodic slots along the z-axis were deployed at different locations as Loc1, Loc3, and Loc5. We considered the line-of-sight and reflected paths here for our measurements. The height of Rx was fixed as 1.6 m along the y-axis. In order to take vertical polarization firstly into account, the receiving dipole was placed vertically to the ground of the Nantong tunnel and periodic slots were placed obliquely and symmetrically to the propagation axis of LCXs. For horizontal polarization, the slot structure is considered perpendicular to the LCX axis. The overall electromagnetic field can be acquired by adding the outcomes of all the slots of LCXs using (8). Based on the above description, the empirical distribution function (ECDF) for all measuring locations and for different polarization schemes is shown in Figure 7. In the meantime, ECDF for capacity was calculated by fixing the SNR as 10 dB. Afterwards, analytical results which were conducted using MATLAB software and the experimentally evaluated real-time Nantong results were compared with the WiSE software. The graphical results show resemblance with each other, which validate our findings, and these results are closer to the i.i.d. values. Due to the limited number of receiving antenna arrays, our results show stepped characteristics. From Figure 7, it is evident that region 1 has more stable radiated field and capacity when compared to the other two regions, and in all regions, horizontally polarized LCXs have improved efficiency in terms of capacity and correlation coefficients.

For further investigation of MIMO systems, we considered the Massif Central tunnel in south central France to examine the correlation coefficients for different MIMO systems [32–34]. The straight subway tunnel under test is made up of concrete material, and its cross-section area consists of 3.5 km (length) × 8.6 m (width) × 7.9 m (height). The tunnel was closed throughout all the experiments. This tunnel is also used for analyzing the radio channel propagation characteristics. There are few researches found in literature about Massif Central tunnel by using conventional antennas, but the LCX-based MIMO system approach was not considered so far. We used the 0.8 km long LCXs which were hanging along the z-axis at three different locations from the sidewall of the tunnel. The first location was 2.7 m high from the ground level of the tunnel, the second location was 1.9 m high, and the third location was 1.5 m high from the ground level. The UHA9125D dipole antennas were used as receiving antennas, and the other measuring parameters are equivalent as listed in Table 1. We divided the total 800 m length into three different regions to estimate the correlation coefficients and capacity as region 1, region 2, and region 3.

Each of the regions is 100 m long. LCXs were positioned at 0.2 m away from the sidewall. Region 1 covers area from 0 m to 100 m, region 2 contains area from 350 m to 450 m, and region 3 consists of area from 700 m to 800 m. Initially, we assumed the 2 m distance between two consecutive receivers. For each region, we measured the MIMO channel characteristics at 51 different receiving locations which were at least 4.1 m away from the LCXs and they were 1.6 m high from the ground level as shown in Figure 8. The transmitted power and frequency were adjusted as 20 dBm and 1.8 GHz, respectively. We firstly examined the horizontally polarized LCXs' scenario for the horizontally polarized receiving antennas and then considered the vertically polarized LCXs and receiving antennas at different locations by using Eq. (9). Here, we attained a total of 48 virtual Rx antenna array matrices for each region. Afterward, the same procedure was repeated for the 5 m distance between two consecutive receivers and a total of 18 virtual Rx antenna arrays were acquired for each region. From the results, we revealed the trend of overall decrement of correlation as a function of receiving locations or number of virtual receiving antenna arrays. We discovered that the 5 m distance assumption between each pair of receiving antennas is favorable than the 2 m separation distance in order to obtain less correlation coefficients. After the decorrelation limit (2λ), the distance among the receivers has very less influence on correlation [35]. As 2 m and 5 m distances are much longer than the decorrelation limit, they have less impact on correlation. Therefore, in region 1 and region 2, both separating distances among receivers show almost similar behavior in Figure 9, but in region 3, the 5 m separation has improved performance than the 2 m separating distance, and the mean value of correlation coefficients' relation is given in Table 2. We also perceived that the horizontally polarized LCX-based

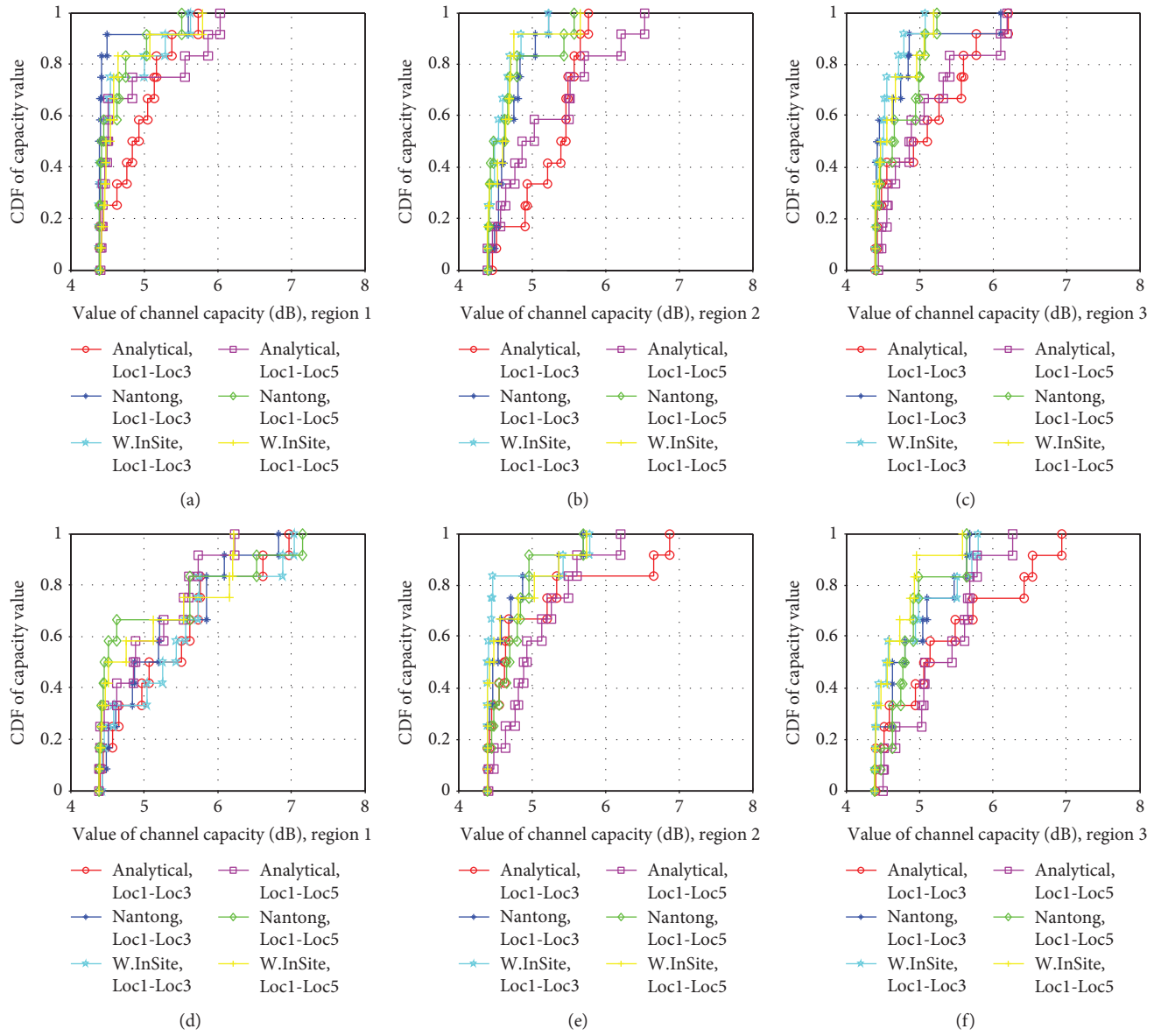

Figure 7: The ECDF comparison for 2 × 2 LCX-based MIMO systems for vertically polarized LCXs for region 1, region 2, and region 3 (a–c) and for horizontally polarized LCXs for region 1, region 2, and region 3 (d–f).

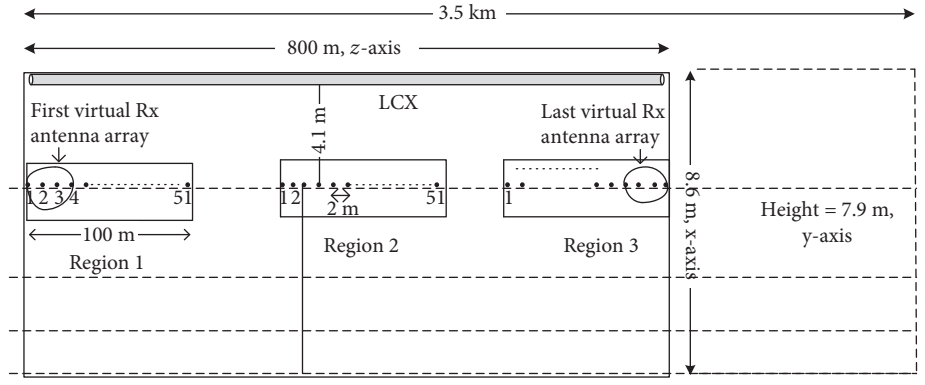

Figure 8: The different measuring locations of the Massif Central tunnel in south central France.

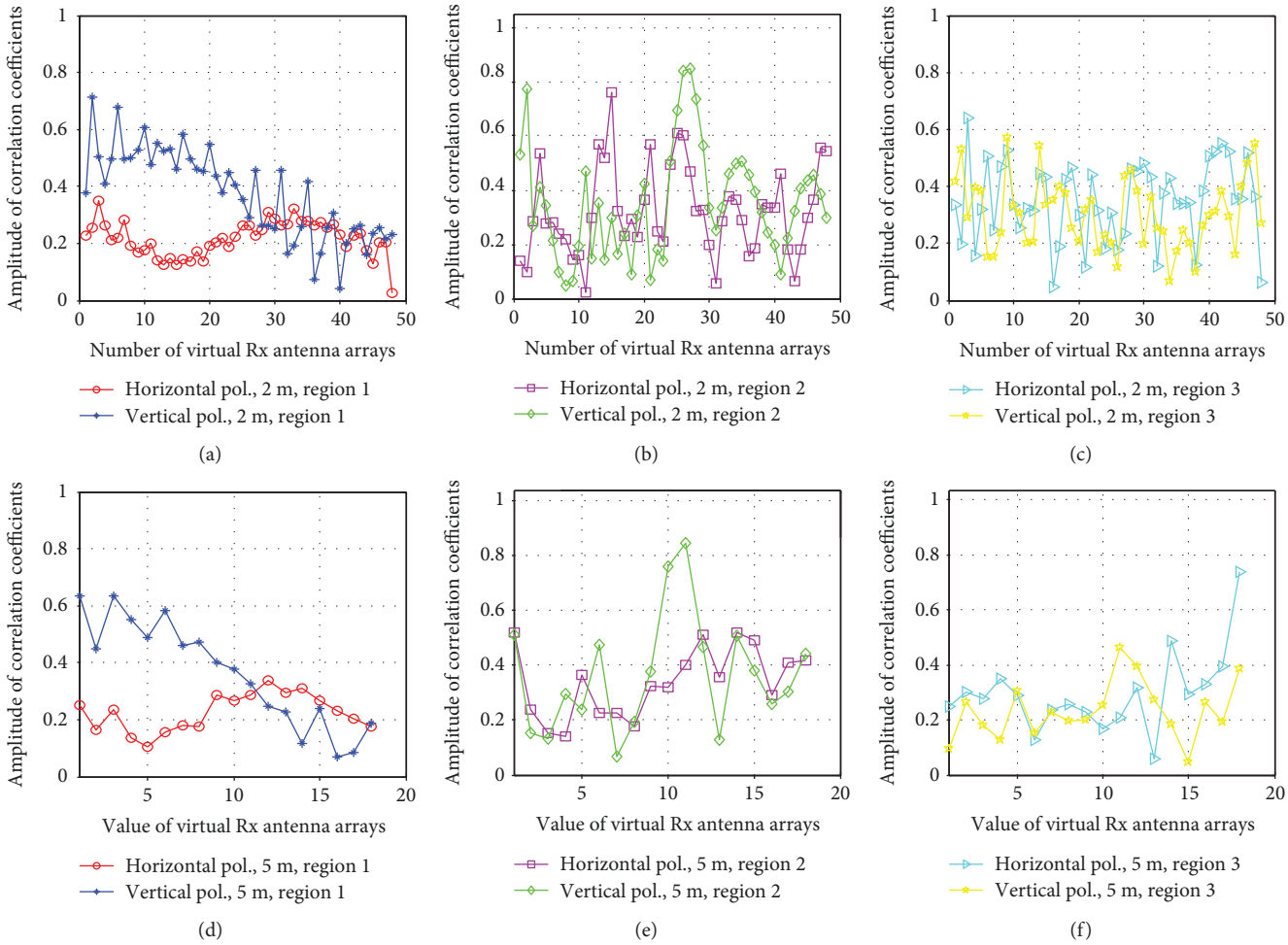

Figure 9: The correlation coefficients for vertically and horizontally polarized LCX-based 3 × 4 MIMO system for the 2 m distance between the Rxs in region 1, region 2, and region 3 (a–c) and for the 5 m distance between the Rxs in region 1, region 2, and region 3 (e–f).

Table 2: The mean value of correlation coefficients for the 2 m and 5 m separation distances.

Separation distance	Polarization type	Region 1	Region 2	Region 3
2 m	Horizontal	0.22	0.32	0.35
	Vertical	0.38	0.35	0.30
5 m	Horizontal	0.23	0.34	0.30
	Vertical	0.36	0.36	0.23

MIMO system depicts less correlation than the vertically polarized LCXs as given in Figure 9.

The empirical distribution function (ECDF) of the capacity for the Massif Central tunnel was further examined for the fixed SNR of 10 dB and the 1.8 GHz frequency by utilizing Eq. (10) for both the 2 m and 5 m separation distance suppositions. From the results, we acknowledged that the horizontally polarized LCX-based 3 × 4 MIMO system depicts improved capacity than the vertically polarized system in all regions for both the 2 m and 5 m separating distance scenarios as prescribed in Figure 10.

Afterward, we estimated the capacity gain for the 2 × 2 LCX-based MIMO system (Loc1 and Loc3) in the Massif Central tunnel and further compared it with the 3 × 4 MIMO system. We divided the measuring campaign into two cases. In the first case, we measured the capacity gain for 1 λ value and then calculated it for the half-lambda (0.5 λ) value in the second case. The total length of the measurement distance in each region was considered only 3 m. It is obvious from the obtained results that the 3 × 4 MIMO system outperforms the 2 × 2 MIMO system and the capacity gain of the 3 × 4 MIMO system is quite closer to the i.i.d. case as given in Tables 3 and 4.

By using Figures 5–10, it can be seen that separations between the antennas and the length of LCXs have significant influence on the performance of MIMO system; so by proper selection of these parameters, a stable and reliable performance can be achieved which is essential for underground radio communication. We also demonstrate that horizontally polarized MIMO systems based on LCXs have favorable performance than the vertically polarized systems for both assumed circumstances.

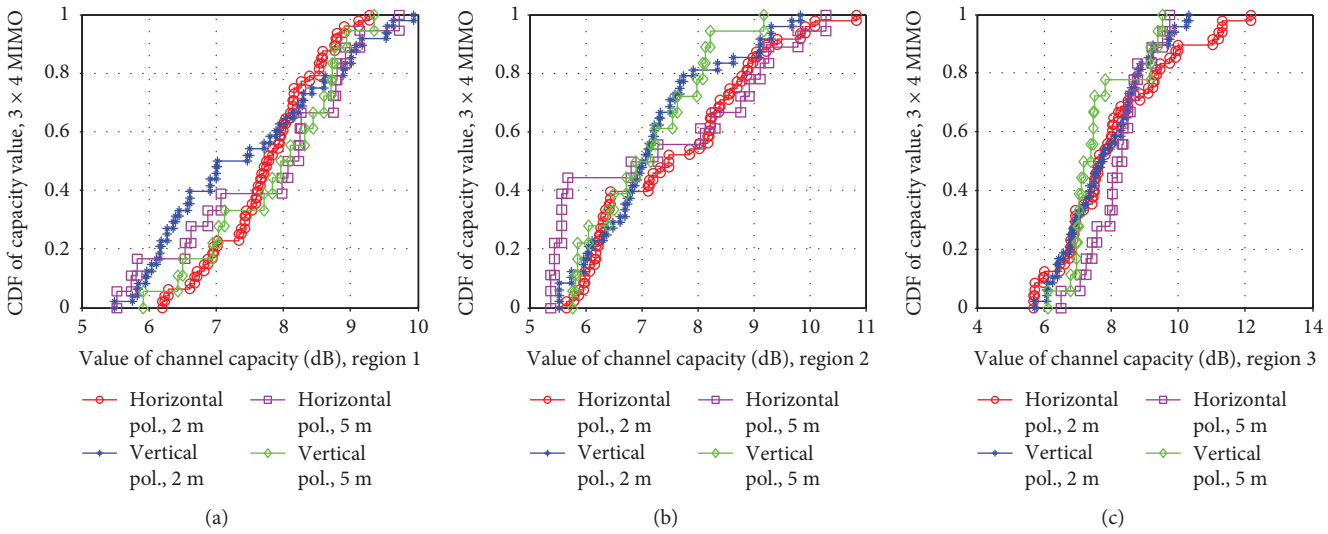

Figure 10: The ECDF comparison of capacity for 3 × 4 LCX-based MIMO systems for the vertically and horizontally polarized LCXs in the Massif Central tunnel for the 2 m and 5 m distances between two consecutive receivers in region 1 (a), region 2 (b), and region 3 (c).

Table 3: The mean value of capacity for the lambda (λ) value distance between the Rx antennas.

Polarization	Massive tunnel, 3 × 4 MIMO			Massive tunnel, 2 × 2 MIMO		
	Region 1	Region 2	Region 3	Region 1	Region 2	Region 3
Horizontal	6.0501	7.6854	6.4409	5.6440	6.2031	5.8050
Vertical	5.6305	5.8452	5.7363	5.5716	5.5629	5.4603

Table 4: The mean value of capacity for the half-lambda (0.5 λ) value distance between the Rx antennas.

Polarization	Massive tunnel, 3 × 4 MIMO			Massive tunnel, 2 × 2 MIMO		
	Region 1	Region 2	Region 3	Region 1	Region 2	Region 3
Horizontal	6.6213	6.7603	6.2468	5.4893	5.8439	5.7145
Vertical	5.5483	5.8283	5.5026	5.4658	5.4584	5.4062

5. Conclusion

This paper studies the LCX-based MIMO systems' measurement campaign in a tunnel environment based on radiated theory and ray tracing method at 1.8 GHz. In order to realize the 2 × 2 MIMO channel performance in the Nantong tunnel, we carried out extensive measurements by using different polarization schemes and by selecting different locations of transmitting and receiving antennas for calculating the channel received powers, channel correlation coefficients, and channel capacities. The separation between LCXs, receiving antenna characteristics, and, moreover, different heights of LCX has substantial impact on the performance of the channel, so that the maximum efficiency can be achieved by properly adjusting these parameters. In all cases, horizontally polarized LCXs have better efficiency than the vertically polarized LCXs, and in region 1, there exists more stable and reliable capacity than in the other regions for the Nantong tunnel scenario. In the Massif Central tunnel case, horizontally polarized 3 × 4 MIMO system exhibits less correlation than vertically polarized system due to different polarization properties and 3 × 4 MIMO systems have improved performance than 2 × 2 MIMO systems. From these results, we can determine that LCX-based MIMO channels have favorable performance for indoor scenarios like tunnels. As a consequence, this paper provides a much more efficient model for an optimum system design and it delivers better direction for the LTE-M systems by means of LCX deployment in the tunnel.

Data Availability

The measurement data used to support the findings of this study have not been made available because of the protection of intellectual property rights. Moreover, the data are shared with our partner company and will be used in our future work. Also, the measurement work costs a lot of manpower and equipment.

Conflicts of Interest

The authors declare that they have no conflicts of interest.

Acknowledgments

This work was supported by the National Natural Science Foundation of China under Grants 61571282 and 61871261 and a fund from the Shanghai Cooperative Innovation Center for Maglev and Rail Transit.

References

[1] N. Nakamura, H. Tsunomachi, and R. Fukui, "Road vehicle communication system for vehicle control using leaky coaxial cable," *IEEE Communications Magazine*, vol. 34, no. 10, pp. 84–89, 1996.

[2] S. Schwarz and M. Rupp, "Society in motion: challenges for LTE and beyond mobile communications," *IEEE Communications Magazine*, vol. 54, no. 5, pp. 76–83, 2016.

[3] D. Li and J. Wang, "Effect of antenna parameters on the field coverage in tunnel environments," *International Journal of Antennas and Propagation*, vol. 2016, Article ID 8180124, 10 pages, 2016.

[4] H. Wang, F. R. Yu, and H. Jiang, "Modeling of radio channels with leaky coaxial cable for LTE-M based CBTC systems," *IEEE Communications Letters*, vol. 20, no. 5, pp. 1038–1041, 2016.

[5] X. Wang, J. Wang, Z. Zhang, and M. Chen, "Coupling characteristics between leaky coaxial cables with and without obstacle," in *2012 10th International Symposium on Antennas, Propagation & EM Theory (ISAPE2012)*, pp. 612–615, Xian, China, 2012.

[6] D. G. Dudley, S. F. Mahmoud, M. Lienard, and P. Degauque, "On wireless communication in tunnels," in *2007 IEEE Antennas and Propagation Society International Symposium*, pp. 3305–3308, Honolulu, HI, USA, 2007.

[7] J. Medbo and A. Nilsson, "Leaky coaxial cable MIMO performance in an indoor office environment," in *2012 IEEE 23rd International Symposium on Personal, Indoor and Mobile Radio Communications - (PIMRC)*, pp. 2061–2066, Sydney, NSW, Australia, 2012.

[8] J. H. Wang and K. K. Mei, "Theory and analysis of leaky coaxial cables with periodic slots," *IEEE Transactions on Antennas and Propagation*, vol. 49, no. 12, pp. 1723–1732, 2001.

[9] F. Mani, F. Quitin, and C. Oestges, "Directional spreads of dense multipath components in indoor environments: experimental validation of a ray-tracing approach," *IEEE Transactions on Antennas and Propagation*, vol. 60, no. 7, pp. 3389–3396, 2012.

[10] M. J. Calderon Jimenez, K. Arana, and M. R. Arias, "Outdoor-to-indoor propagation mechanisms in multistorey building for 0.85 GHz and 1.9 GHz bands," in *2017 IEEE 37th Central America and Panama Convention (CONCAPAN XXXVII)*, pp. 1–6, Managua, Nicaragua, 2017.

[11] K. Guan, B. Ai, B. Peng et al., "Towards realistic high-speed train channels at 5G millimeter-wave band—part I: paradigm, significance analysis, and scenario reconstruction," *IEEE Transactions on Vehicular Technology*, vol. 67, no. 10, pp. 9112–9128, 2018.

[12] K. Guan, D. He, B. Ai et al., "5-GHz obstructed vehicle-to-vehicle channel characterization for internet of intelligent vehicles," *IEEE Internet of Things Journal*, 2018.

[13] X. Chen, "Antenna correlation and its impact on multiantenna system," *Progress In Electromagnetics Research B*, vol. 62, pp. 241–253, 2015.

[14] Y. Hou, S. Tsukamoto, S. Li, T. Higashino, K. Kobayashi, and M. Okada, "Capacity evaluation of MIMO channel with one leaky coaxial cable used as two antennas over linear-cell environments," *IEEE Transactions on Vehicular Technology*, vol. 66, no. 6, pp. 4636–4646, 2017.

[15] X. Zhang, X. Yang, L. Guo, and Z. Zhao, "Research on the radiated field's distribution of leaky coaxial cable in the blind zone," in *2006 1st International Symposium on Systems and Control in Aerospace and Astronautics*, pp. 4–7, Harbin, China, 2006, IEEE.

[16] Z. Zhao, X. Yang, and S. Guo, "A coupling loss algorithm of leaky coaxial cable in the blind zone," in *2008 IEEE International Conference on Mechatronics and Automation*, pp. 919–923, Takamatsu, Japan, 2008.

[17] J. Wang, Y. Li, Z. Zhang, and M. Chen, "Radiation field computation of leaky coaxial cables by finite-difference time domain in cylindrical coordinates and equivalent source integration," *IET Microwaves, Antennas & Propagation*, vol. 5, no. 14, pp. 1756–1762, 2011.

[18] A. Saleem, M. Wang, and G. Zheng, "Scattering of electric field from leaky coaxial cable in confined area," *International Journal of Antennas and Propagation*, vol. 2017, Article ID 2894397, 9 pages, 2017.

[19] P. Kyritsi, D. C. Cox, R. A. Valenzuela, and P. W. Wolniansky, "Correlation analysis based on MIMO channel measurements in an indoor environment," *IEEE Journal on Selected Areas in Communications*, vol. 21, no. 5, pp. 713–720, 2003.

[20] S. Bashir, "Effect of antenna position and polarization on UWB propagation channel in underground mines and tunnels," *IEEE Transactions on Antennas and Propagation*, vol. 62, no. 9, pp. 4771–4779, 2014.

[21] I. B. Mabrouk, J. Hautcoeur, L. Talbi, M. Nedil, and K. Hettak, "Feasibility of a millimeter-wave MIMO system for short-range wireless communications in an underground gold mine," *IEEE Transactions on Antennas and Propagation*, vol. 61, no. 8, pp. 4296–4305, 2013.

[22] W. Q. Malik, "Spatial correlation in ultrawideband channels," *IEEE Transactions on Wireless Communications*, vol. 7, no. 2, pp. 604–610, 2008.

[23] A. E. Forooshani, R. D. White, and D. G. Michelson, "Effect of antenna array properties on multiple-input–multiple-output system performance in an underground mine," *IET Microwaves, Antennas & Propagation*, vol. 7, no. 13, pp. 1035–1044, 2013.

[24] M. Lienard, P. Degauque, J. Baudet, and D. Degardin, "Investigation on MIMO channels in subway tunnels," *IEEE Journal on Selected Areas in Communications*, vol. 21, no. 3, pp. 332–339, 2003.

[25] F. P. Fontán and P. M. Espiñeira, *Modeling the Wireless Propagation Channel: A Simulation Approach with MATLAB*, John Wiley & Sons, Ltd, 2008.

[26] I. Khan and P. S. Hall, "Experimental evaluation of MIMO capacity and correlation for narrowband body-centric wireless channels," *IEEE Transactions on Antennas and Propagation*, vol. 58, no. 1, pp. 195–202, 2010.

[27] N. Jamaly, R. Merz, A. Schumacher, D. Scanferla, and D. Wenger, "MIMO capacity enhancement beyond that of the ideal Rayleigh multipath by virtue of a leaky feeder cable," in *2016 10th European Conference on Antennas and Propagation (EuCAP)*, pp. 1–5, Davos, Switzerland, 2016.

[28] J. Weng, X. Tu, Z. Lai, S. Salous, and J. Zhang, "Indoor massive MIMO channel modelling using ray-launching simulation," *International Journal of Antennas and Propagation*, vol. 2014, Article ID 279380, 13 pages, 2014.

[29] Y. Jiang, G. Zheng, X. Yin, A. Saleem, and B. Ai, "Performance study of millimetre-wave MIMO channel in subway tunnel using directional antennas," *IET Microwaves, Antennas & Propagation*, vol. 12, no. 5, pp. 833–839, 2018.

[30] S. J. Fortune, D. M. Gay, B. W. Kernighan, O. Landron, R. A. Valenzuela, and M. H. Wright, "WISE design of indoor wireless systems: practical computation and optimization," *IEEE Computational Science and Engineering*, vol. 2, no. 1, pp. 58–68, 1995.

[31] M. J. C. Jimenez, K. Arana, and M. R. Arias, "Outdoor-to-indoor propagation mechanisms in multistorey building for 0.85 GHz and 1.9 GHz bands," in *2017 IEEE 37th Central America and Panama Convention (CONCAPAN XXXVII)*, pp. 1–6, Managua, Nicaragua, 2017.

[32] D. G. Dudley, M. Lienard, S. F. Mahmoud, and P. Degauque, "Wireless propagation in tunnels," *IEEE Antennas and Propagation Magazine*, vol. 49, no. 2, pp. 11–26, 2007.

[33] S. F. Mahmoud, "Wireless transmission in tunnels with non-circular cross section," *IEEE Transactions on Antennas and Propagation*, vol. 58, no. 2, pp. 613–616, 2010.

[34] X. Zhang and C. D. Sarris, "A Gaussian beam approach for embedding antennas into vector parabolic equation based propagation models," in *2016 IEEE International Symposium on Antennas and Propagation (APSURSI)*, pp. 2105-2106, Fajardo, Puerto Rico, 2016, IEEE.

[35] Y. S. Cho, J. Kim, W. Y. Yang, and C. G. Kang, *MIMO-OFDM Wireless Communications with MATLAB®*, John Wiley & Sons, 2010.